

Evaluation of Diffracted Wavefields Below the Salt Stringer Using the Transmission-Propagation Operator Theory and TWSM Software Package

Nikolay Zyatkov
Novosibirsk State University
Novosibirsk, Russia
nikolay.zyatkov@gmail.com

Alena Ayzenberg
University of Bergen
Bergen, Norway
alena.ayzenberg@uib.no

Kamaldeen Omosanya
NTNU
Trondheim, Norway
kamaldeen.o.omosanya@ntnu.no

Alexey Romanenko
Novosibirsk State University
Novosibirsk, Russia
arom@ccfit.nsu.ru

Arkady Aizenberg
IPPG SB RAS
Novosibirsk, Russia
AizenbergAM@ipgg.sbras.ru

ABSTRACT

We consider a seismic salt stringer image. The interpretation in the shadow zone beneath the stringer has complications due to that the diffracted and transmitted wavefields destructively interfere causing poor image. For simulating the real image we evaluate seismic wavefields in the shadow zone by combining the transmission-propagation operator theory (TPOT) and the tip-wave superposition method (TWSM) which is a mid-frequency range approximation of TPOT. This mathematical model has a layer with two flat boundaries, one of which has a dense coin-shaped addition reminding an anhydrite disk. We propose analytical separation of the wavefield below the stringer by TPOT and its computation by the TWSM software package. We describe usage of GPU-cluster to accelerate modeling and give an estimated time of wavefields simulation for stringer model.

Categories and Subject Descriptors

H.4 [Information Systems Applications]: Miscellaneous;
G.1.0 [Numerical analysis]: Parallel algorithms

General Terms

Theory, Algorithms, Performance

Keywords

seismic modeling, HPC, GPU

1. INTRODUCTION

Seismic interpretation beneath salt stringers is often complicated due to the difference in the physical and acoustic

properties of the salt/evaporate and the stringers. Intra-salt deformation has been the focus of the oil and gas industries, and the academia in the last two decades [6], [7], [4]. Salt floaters are important reservoir rocks and geological storage in NW Europe and in the South Oman Salt Basin [5]. Apart from their economic importance, overpressure associated with salt stringers is drilling hazards, which are often hard to predict. The diffracted and transmitted wavefields in the shadow destructively interfere causing poor seismic imaging. There are several heuristic methods that separate primary reflections, surface-related multiples and internal multiples from the total wavefield in acoustic and elastic media [8]. We suggest the analytical separation from the total wavefield in multiphysics (acoustic, elastic, porous, fluid-saturated, etc.) block-layered media for the first time.

In this paper, we use the transmission-propagation operator theory (TPOT) to describe the acoustic blanking or shadow zone beneath a salt stringer in order to mitigate drilling hazards and provide better imaging of the intra-salt reservoir rocks. For simulating the real image we evaluate wave fragments of the interference wavefields into the shadow zone by highly-optimized software package based on the tip-wave superposition method (TWSM) that is a mid-frequency approximation of TPOT. We show usage of GPU-cluster to accelerate modeling by the TWSM package and give an estimated time of wavefields simulation for stringer model.

2. SALT STRINGER IMAGE AND ITS MATHEMATICAL MODEL

We consider a salt stringer image (Figure 1). By black ellipse, we emphasized the stringer part, which causes shadow beneath it and leads to this poor image. We aim to separate the wavefield in the shadow zone for better 'illumination'. Additionally, we consider a mathematical model (Figure 2) representing a large-scale picture of the stringer on Figure 1. This model consists of Sediments 1 and 2, Halite 1 and 2 and a thin Anhydrite disk. The interfaces have coordinate $z = -3.3$ km, $z = -4.0$ km and $z = -4.6$ km, respectively. The thickness of Anhydrite disk is ~ 0.042 km in length with a radius of 0.5 km. Sediments 1 and 2 have ve-

Permission to make digital or hard copies of all or part of this work for personal or classroom use is granted without fee provided that copies are not made or distributed for profit or commercial advantage and that copies bear this notice and the full citation on the first page. To copy otherwise, to republish, to post on servers or to redistribute to lists, requires prior specific permission and/or a fee.

ICAIT '16, Oct. 6 – 8, 2016, Aizu-Wakamatsu, Japan.
Copyright 2016 University of Aizu Press.

locity of 2.5 km/sec and density of 2.5 g/cm³, respectively. Halite 1 and 2 have velocity of 4.5 km/sec and density of 2.2 g/cm³. Anhydrite disk has velocity of 6.5 km/sec and density of 2.9 g/cm³. A source is located in Sediments 1 at point: ($x = 0$ km, $y = 0$ km, $z = 0$ km). The source radiates a spherical P-wave represented by the scalar potential satisfying the Helmholtz equation. The wavelet is given by formula $e^{-(2\tau)^2} \cos(2\pi\tau)$, where $\tau = t/T - 2$, $T = 0.032$ s and dominant frequency 38.25 Hz. A 20 receivers array is spread in Sediments 1 along the line: ($x = -1.0$ to 0.9 km with the step $\Delta x = 0.1$ km, $y = 0$ km, $z = 0$ km). We consider two wave codes: reflection from Anhydrite disk (C1) and reflection from the bottom salt (C2) (Figure 2).

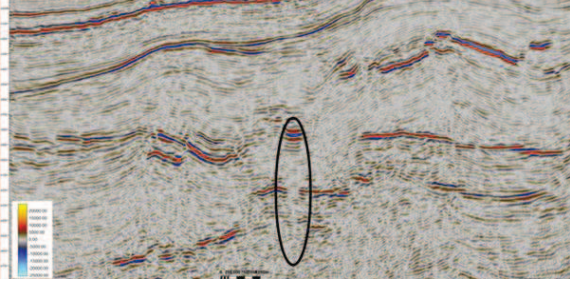


Figure 1: An example of a salt stringer, the Norwegian North Sea.

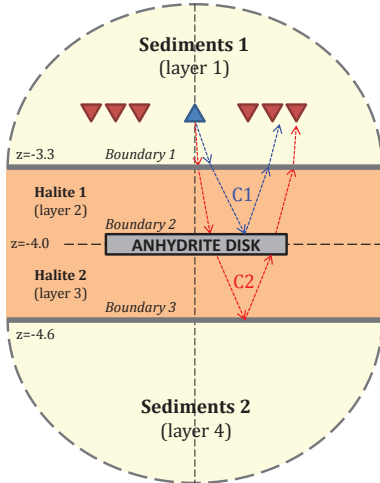


Figure 2: 3D mathematical stringer model.

3. TPOT&TWSM APPROACH IN SALT STRINGER MODEL

TPOT describes in explicitly analytic form propagation of the seismic wavefields in 3D block-layered geologic media by action of two operators: 1) transmission operator (reflection/refraction) \mathbf{T} at curved interface, 2) propagation operator \mathbf{P} inside block/layer [1], [2]. TPOT can evaluate not only the total wavefield but also structure of the feasible wave fragments in layered and macro-block media. Tip-wave superposition method (TWSM) being the mid-frequency range approximation of TPOT evaluates sequential action of composite operators \mathbf{TP} in layers in according with the chosen

wave code on the wave amplitude functions \mathbf{a} . Operators \mathbf{TP} are approximated by layer matrices, and functions \mathbf{a} – by layer vectors. Scalar elements of matrices and vectors are represented by analytical formulae [9].

TWSM evaluates the wave amplitude functions \mathbf{a}^x by multiple multiplication of large scale matrices \mathbf{P} and \mathbf{T} and wave amplitude function \mathbf{a}^{s_1} for source wavefield at interface \mathbb{S}_1 . For stringer model wave amplitude function with wave code C1 at receiver can be represented as matrix-vector multiplication:

$$\mathbf{a}^x = \mathbf{P}^{x s_1} \cdot \mathbf{T}_{12} \cdot \mathbf{P}^{s_1 s_2} \cdot \mathbf{T}_{23} \cdot \mathbf{P}^{s_2 s_1} \cdot \mathbf{T}_{21} \cdot \mathbf{a}^{s_1} \quad (1)$$

Wave amplitude function with wave code C2 at receiver can be represented as:

$$\mathbf{a}^x = \mathbf{P}^{x s_1} \cdot \mathbf{T}_{12} \cdot \mathbf{P}^{s_1 s_2} \cdot \mathbf{T}_{23} \cdot \mathbf{P}^{s_2 s_3} \cdot \mathbf{T}_{34} \cdot \mathbf{P}^{s_3 s_2} \cdot \mathbf{T}_{32} \cdot \mathbf{P}^{s_2 s_1} \cdot \mathbf{T}_{21} \cdot \mathbf{a}^{s_1} \quad (2)$$

Matrices $\mathbf{P}^{s_j s_i}$ describe propagation from elements of interface i to elements of interface j . Matrix $\mathbf{P}^{x s_1}$ describes propagation from elements of interface \mathbb{S}_1 to receiver x . Matrices \mathbf{T}_{kl} describe transmission from layer l in layer k . Matrices \mathbf{T}_{23} in (1) and \mathbf{T}_{34} in (2) describe reflections, other matrices \mathbf{T}_{kl} describe refractions.

4. TWSM SOFTWARE PACKAGE

TWSM software package is highly-optimized realization of the TWSM for acoustic case adapted for GPU-cluster. Necessity to storage and process large scale matrices and vectors is a main problem of realization of the TWSM. Each interface of layered medium is triangulated by N triangles, each matrix of type 'interface - interface' is square and has dimension $N \times N$. Matrix of type 'interface - receiver' has dimension $M \times N$, where M is number of receivers. Wave amplitude vector of type 'source - interface' has dimension $N \times 1$. Each wave amplitude vector in the frequency domain demands to repeat matrix-vector multiplications (1) and (2) for each discrete frequency ω_k of some frequency array $\omega_1 \dots \omega_K$. Acceleration of each matrix-vector multiplication is realized by GPU-cluster with help of scheme, shown at Figure 3. Each GPU accelerator processes multiplication of group of matrix strips corresponding to frequencies $\omega_1 \dots \omega_K$ by group of wave amplitude vectors. Finally GPUs gather new transformed group of wave amplitude vectors via exchange by evaluated data. Since matrix dimension is $N \sim 10^5 - 10^6$, then TWSM software package can potentially keep any number of available GPUs but no more than N . Curve of scalability the TWSM software package is demonstrated at Figure 4.

5. TWSM COMPUTATION RESULTS FOR CODES C1 AND C2

For the computation of codes C1 and C2, we use formulae (1) and (2) with the transmission operators \mathbf{T} and propagation operators \mathbf{P} . We approximate the transmission operators at interfaces 'Sediments1 - Halite1' and 'Halite2 - Sediments2' in these formulae by the plane-wave transmission (reflection/refraction) coefficients. The interface 'Halite1 - Halite2' has no contrast. For the thin Anhydrite disk with thickness Δz the transmission (reflection/refraction) coeffi-

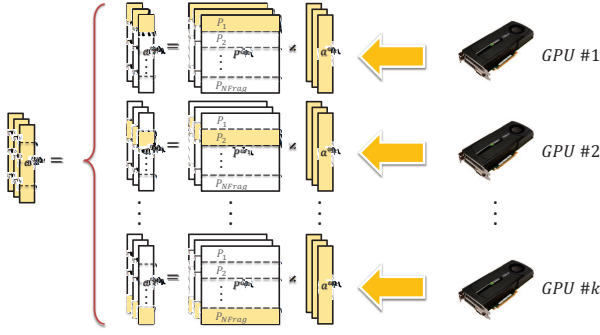


Figure 3: TWSM matrix-vector multiplication scheme adapted for GPU-cluster.

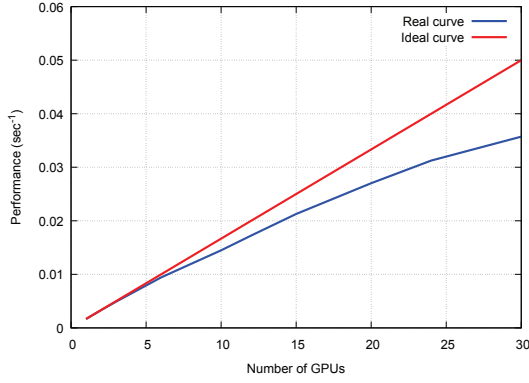


Figure 4: Scalability of TWSM software package.

cients of thin layer are [3]

$$R_{Disk} = T_{22} \frac{1 - e^{i2\pi 2\Delta \bar{z}}}{1 - e^{i2\pi 2\Delta \bar{z}} T_{22}^2}, T_{Disk} = \frac{(1 - T_{22}^2) e^{i2\pi \Delta \bar{z}}}{1 - e^{i2\pi 2\Delta \bar{z}} T_{22}^2}$$

In Anhydrite disk we have the dominant wave period $T_{dom} = \frac{1}{38.25 Hz} = 0.026$ s, the dominant wavelength $\lambda_{dom} = 6.5$ km/s * 0.026 s = 0.169 km, the thickness normalized by the wavelength $\bar{z} = \Delta z / \lambda_{dom} = 0.042 / 0.169 \approx 0.25$ and $e^{i2\pi 2\Delta \bar{z}} = e^{2\pi} = -1$. Halite - Anhydrite reflection at 0 degree is $T_{22} = (1/z_2 - 1/z_3) / (1/z_2 + 1/z_3) \approx 0.3113$, acoustic impedance for Halite is $z_2 = v_{P2} * \rho_2 = 4.5 * 2.2 = 9.9$ and acoustic impedance for Anhydrite is $z_3 = v_{P3} * \rho_3 = 6.5 * 2.9 = 18.85$. The reflection and transmission coefficients from Anhydrite disk are hence computed as follows

$$R_{Disk} \approx 0.567, T_{Disk} \approx 0.823 e^{i\frac{\pi}{2}} \approx 0.823 \frac{1+i}{\sqrt{2}}$$

Codes C1 (the upper curve) and C2 (the lower curve) are represented on Figure 5. Code C1 has stable and strong pulse shape, while code C2 has unstable and weak pulse shape. The change in the pulse shape is caused by the interference of the transmitted and diffracted wavefields. To better 'illuminate' the sub-stringer zone, we need to consider code C2 separately (Figure 6). The pulse of code C2 can be analyzed by removing Anhydrite disk (Figure 7). The difference between the seismograms on Figures 6 and 7 is illustrated on Figure 8, which gives understanding of the diffraction wavefield which we intend to remove from the

whole modeling to get better 'illumination'.

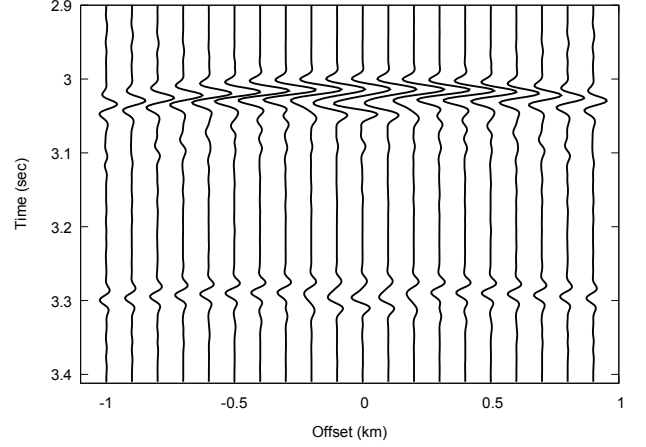


Figure 5: Codes C1 and C2.

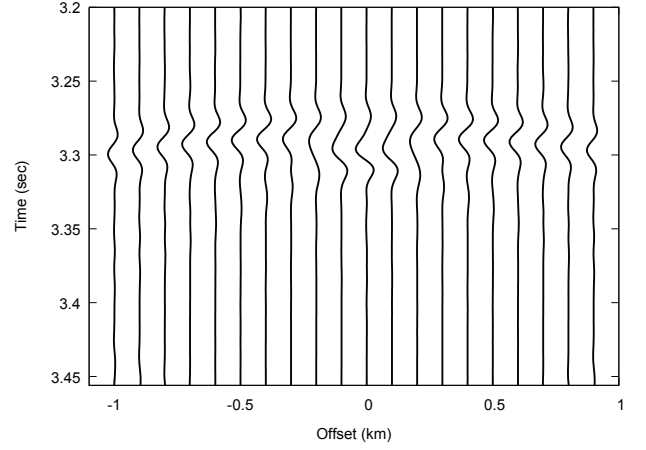


Figure 6: Separated code C2 from the common seismogram on Figure 5.

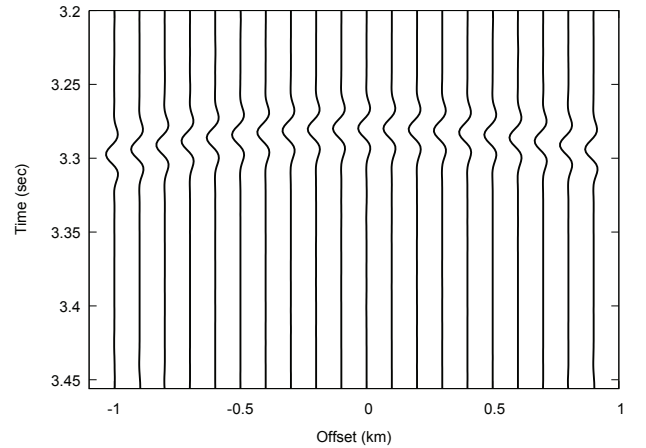


Figure 7: Code C2 with absence of Anhydrite disk.

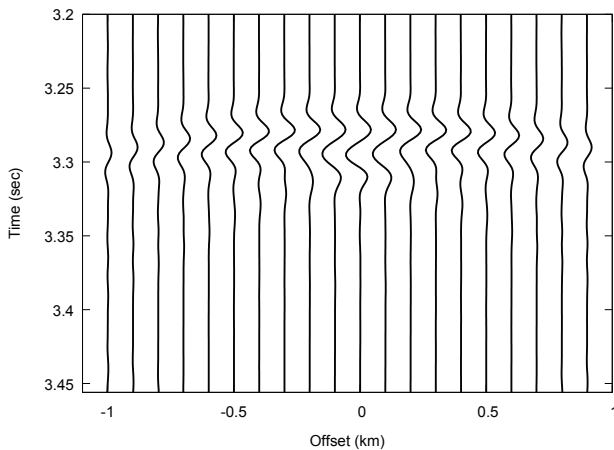


Figure 8: Difference of codes C2 with and without Anhydrite disk.

6. PERFORMANCE ANALYSIS OF TWSM FOR CODES C1 AND C2

Time of multiplication on 12 GPUs K layer matrices with dimension $N \times N$ and K wave amplitude vectors with dimension $N \times 1$ as function of number of triangles N at interface is shown in Table 1. We assume value $K = 128$ that corresponds to 128 discrete frequencies and time window 0.512 sec at seismograms. To decrease time of evaluation we apply rough approximation of the transmission operator with help of the plane-wave reflection/refraction coefficients. Let us estimate computational time of matrix-vector multiplication for wave codes C1 and C2 by formulae (1) and (2). In numerical tests each interface is triangulated by $N = 100000$ elements. We can neglect with computational time of evaluation of matrix 'interface - receivers' since it has dimension $M \times N$ when $M \ll N$. Using Table 1 we can obtain the calculation time for wave code C1 which will be $t = t_{P^2s_1} + t_{P^1s_2} = 38 + 38 = 76$ sec on 12 GPUs. Time calculation for wave code C2 will be $t = t_{P^2s_1} + t_{P^3s_2} + t_{P^2s_3} + t_{P^1s_2} = 38 + 38 + 38 + 38 = 152$ sec on 12 GPUs. For decreasing of computation time for wave codes C1 and C2 we can increase the number of involved GPUs in the TWSM software package.

Table 1: Time of filling and multiplication of group of square matrices and vectors as function of their dimension

Matrix dimensional (N)	Calculation time (sec)
10000	1
50000	9
100000	38
105000	83
200000	148
250000	229

7. CONCLUSIONS

In this paper, we consider a salt stringer image. Because the diffracted and transmitted wavefields destructively interfere, the image beneath the stringer is poor. To solve

this problem we do analytical separation of the wavefield in the shadow zone beneath the stringer by TPOT and evaluate wavefields by highly-optimized TWSM software package adapted for GPU-cluster. This separation allows using only transmitted (or only diffracted) wavefield in evaluation and imaging, which will provide better 'illumination' of the shadow zone. The separated wavefield is obtained for a mathematical model simulating the stringer image. This mathematical model is a large scale sketch of the salt stringer. The separated wavefield is given in form of seismogram. The impact of stringer diffraction is presented on a separate seismogram.

8. ACKNOWLEDGMENTS

We are thankful to NTNU and the Research Centres Bergen and Trondheim of Statoil ASA. We thank Milana Ayzenberg, Jan Pajchel, Ola-Petter Munkvold, Alexey Stovas and Kees Wapenaar.

9. REFERENCES

- [1] A. Aizenberg and A. Ayzenberg. Feasible fundamental solution of the multiphysics wave equation in inhomogeneous domain of complex shape. *Wave Motion*, 53:66–79, March 2015.
- [2] A. Aizenberg, N. Zyatkov, A. Ayzenberg, and E. Rakshaeva. New concepts of the transmission-propagation operator theory in seismic diffraction modeling and interpretation. *76th EAGE Conference and Exhibition*, pages We-P06–07, June 2014.
- [3] L. Brekhovskikh. *Waves in Layered Media*. New York: Academic Press, 1960.
- [4] H. V. Gent, S. Back, J. Urai, and P. Kukla. Small-scale faulting in the upper cretaceous of the groningen block (the netherlands): 3d seismic interpretation, fault plane analysis and regional paleostress. *Journal of Structural Geology*, 32:537–553, April 2010.
- [5] H. V. Gent, J. Urai, and M. de Keijzer. The internal geometry of salt structures - a first look using 3d seismic data from the zechstein of the netherlands. *Journal of Structural Geology*, 33(3):292–311, March 2011.
- [6] Z. Gvirtzman, M. Reshef, O. Buch-Leviatan, and Z. Ben-Avraham. Intense salt deformation in the levant basin in the middle of the messinian salinity crisis. *Earth and Planetary Science Letters*, 379:108–119, October 2013.
- [7] C.-L. Jackson, M. Jackson, M. Hudec, and C. Rodriguez. Enigmatic structures within salt walls of the santos basin - part 1: Geometry and kinematics from 3d seismic reflection and well data. *Journal of Structural Geology*, 75:135–162, June 2015.
- [8] Y. Liu, H. Hu, X.-B. Xie, Y. Zheng, and P. Li. Reverse time migration of internal multiples for subsalt imaging. *Geophysics*, 80(5):S175–S185, September 2015.
- [9] N. Zyatkov, A. Ayzenberg, A. Aizenberg, and A. Romanenko. Highly-optimized twsm algorithm for modeling cascade diffraction in terms of propagation-absorption matrices. *75th EAGE Conference and Exhibition*, pages Th-P02–11, June 2013.